This is an open access article published under an ACS AuthorChoice License, which permits copying and redistribution of the article or any adaptations for non-commercial purposes.

ACS OMEGA

http://pubs.acs.org/journal/acsodf

Article

Efficient and Environmentally Friendly Adsorbent Based on β-Ketoenol-Pyrazole-Thiophene for Heavy-Metal Ion Removal from Aquatic Medium: A Combined Experimental and Theoretical Study

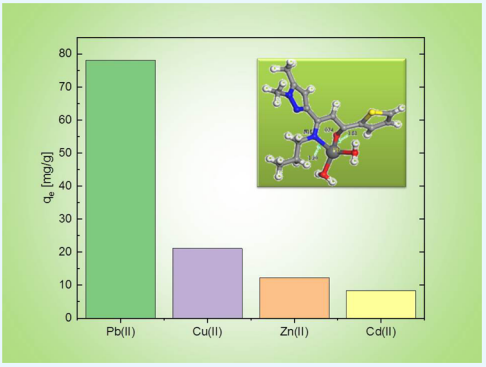
Said Tighadouini,* Smaail Radi,* Mohamed El Massaoudi, Zouhair Lakbaibi, Marilena Ferbinteanu, and Yann Garcia*

Cite This: *ACS Omega* 2020, 5, 17324−17336

Read Online

ACCESS | Metrics & More | Article Recommendations | Supporting Information

ABSTRACT: A new sustainable and environmentally friendly adsorbent based on a β-ketoenol-pyrazole-thiophene receptor grafted onto a silica surface was developed and applied to the removal of heavy-metal ions (Pb(II), Cu(II), Zn(II), and Cd(II)) from aquatic medium. The new material **SiNPz-Th** was well characterized and confirms the success of covalent binding of the receptor on the silica surface. The effect of environmental parameters on adsorption including pH, contact time, temperature, and the initial concentration were investigated. The maximum adsorption capacities of **SiNPz-Th** for Pb(II), Cu(II), Zn(II), and Cd(II) ions were 102.20, 76.42, 68.95, and 32.68 mg/g, respectively, at 30 min and pH = 6. The adsorption isotherms, kinetics, and thermodynamic process were investigated and showed efficiency and selectivity toward Pb(II) and good regeneration performance. Density functional theory, noncovalent-interaction, and quantum theory of atoms in molecules calculations were used to study and to gain a deeper understanding of both the adsorption mechanism and selectivity of metal ions onto the adsorbent. Accordingly, metal ions such as Pb(II), Cu(II), and Zn(II) were bidentate coordinated with the adsorbent by nitrogen and oxygen atoms of the Schiff base C═N and hydroxyl group −OH, respectively, to form stable complexes. Whereas Cd(II) was coordinated in a monodentate fashion with oxygen atom of the hydroxyl group. Furthermore, the affinity of **SiNPz-Th** toward the metal ions was decreased in the order of Pb(II) > Cu(II) > Zn(II) > Cd(II), in good agreement with the experimental results. All these results highlight that **SiNPz-Th** has good potential to be an advanced adsorbent for the removal of lead ions from real water.



INTRODUCTION

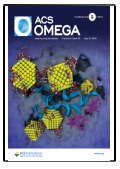
In recent years, extensive industrialization has generated severe environmental problems; water contamination by heavy metals is seriously hazardous to the aquatic environment. These metal ions can cause serious health hazard to humans, even at low concentrations.[1−4] Lead has been identified as one of the toxic elements which can cause serious diseases such as renal disturbances, hepatitis, anemia, cancer, and so forth.[5,6] A wide range of treatment technologies have been indicated for the removal of heavy metals from contaminated water in the last decades, starting from liquid−liquid extraction,[7] ion exchange,[8] chemical precipitation,[9] membrane filtration,[10] coagulation,[11] adsorption,[12−14] and ending with electrochemical treatment.[15] Among these approaches, adsorption is regarded as one of the very popular ones and captures enormous attention due to its high efficiency, simplicity, economy, and high environmental friendliness.[16,17] Hence, several of such adsorbents, such as graphene,[18] bentonite,[19] cellulose,[20] zeolite,[21] and so forth, were fabricated and applied to the elimination of heavy metals in aquatic systems.

Functional silica gel has attracted much interest due to its low-cost, feasibility, high thermal and mechanical stability, and large surface areas.[22,23] In addition, the possibility to introduce various organic ligands onto its surface to construct adsorbents that can effectively trap potential toxic metal ions[24−30] and its adsorption performance, which mainly depends on the nature of grafted ligands, are considered as the key success factors to better chelate with metal ions.[31−33]

In the past decades, several functional groups containing donor atoms, such as nitrogen, oxygen, and sulfur have been employed to construct adsorbents with high efficiency.[34−42]

In this context, pyrazole has received much attention for its highly interesting properties in coordination chemistry,[43,44] particularly for the synthesis of lead complexes.[45,47] On the other hand, β-ketoenol is an interesting compound which is

Received: April 8, 2020
Accepted: June 19, 2020
Published: July 9, 2020

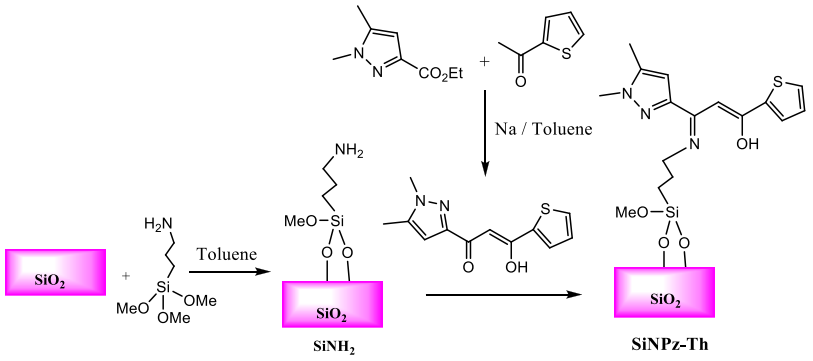


Downloaded via UNIV CATHOLIQUE DE LOUVAIN on July 24, 2020 at 13:07:32 (UTC).
See https://pubs.acs.org/sharingguidelines for options on how to legitimately share published articles.

© 2020 American Chemical Society

https://dx.doi.org/10.1021/acsomega.0c01616
ACS Omega 2020, 5, 17324−17336

Scheme 1. Synthetic Pathway to the Hybrid Material SiNPz-Th



known for its high complexing ability with most transition-metal ions.[48,50]

The reaction of an amine group with a ketone group leads to the formation of a Schiff base which is known for its excellent capacity to coordinate metal complexes.[51−53]

In the present study, an efficient adsorbent based on *β*-ketoenol-pyrazole-thiophene-functionalized silica gel (**SiNPz-Th**) was successfully fabricated and characterized.[46]

The adsorbent can be regarded as a low production cost, simple to prepare, and environmentally friendly means for potentially toxic-metal-ion removal. The impact of pH value, contact time, swelling kinetics, initial concentrations, adsorption isotherm, regeneration time, and selectivity of metal ion in the mixture were discussed and evaluated. On the other hand, density functional theory (DFT), noncovalent-interaction (NCI), and quantum theory of atoms in molecules (QTAIM) methods have been applied to gain a deeper understanding of the adsorption mechanism and selectivity of the metal ion toward the ligand structure.[49]

RESULTS AND DISCUSSION

Linker Synthesis. The fabrication principle of our new adsorbent is shown in Scheme 1. The first stage concerns the preparation of the target (*Z*)-1-(1,5-dimethyl-1*H*-pyrazol-3-yl)-3-hydroxy-3-(thiophen-2-yl)prop-2-en-1-one ligand ($\mathbf{L_1}$) in its stable conjugated enol tautomeric form. The structure of the synthesized ligand was suitable for X-ray, analytical, and spectroscopic studies. The second step involves the preparation of 3-aminopropyl-silica ($\mathbf{SiNH_2}$) by condensation of silica with 3-aminopropyltrimethoxysilane. Finally, the target $\mathbf{L_1}$ molecule was anchored to NH_2-groups to yield the new chelating adsorbent named **SiNPz-Th** (Scheme 1).

L_1 Crystal Structure. The $\mathbf{L_1}$ crystallizes in the orthorhombic system, space group $P2_12_12_1$ (#19). The crystal structure shows a planar structure (Figure 1). The molecule is planar with the O and S atoms located in the same semiplane and the N atom in an anti position. Despite possible conformational degrees of freedom, it is important to note the role of delocalization and conjugation. The *β*-ketoenol moiety has an inner hydrogen bond, which possibly shows dynamic features that may contribute to a disorder that affects the crystal parameters. The planar molecules are arranged in a zig-zag fashion to have a very compact packing.

Characterization Methods. The percentage of carbon, nitrogen, and sulfur contained in $\mathbf{L_1}$ covalently grafted onto silica surface was confirmed by elemental analysis. The hybrid material **SiNPz-Th** showed atomic percentage of C, N, and S of 4.6, 1.94, and 0.2%, respectively.

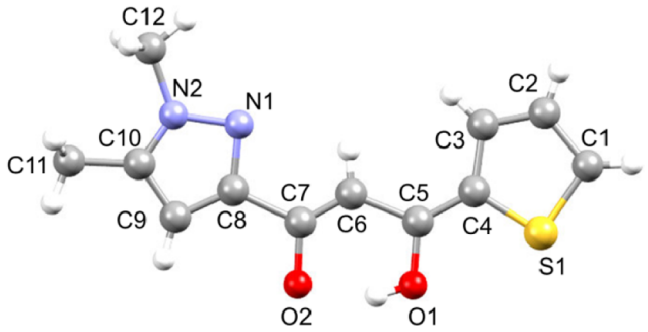


Figure 1. X-ray molecular structure of $\mathbf{L_1}$ with atoms numbering scheme ($\mathbf{L_1}$: a = 4.163(7) Å, b = 14.96(2) Å, c = 19.62(3) Å, V = 1222(3) Å^3. Z = 4; T = 20 °C; D_{calc} = 1.350 g/cm^3; no. of reflections measured total: 7793, unique: 2775; R_1 (I > 2.00σ(I)) 0.1744, R (all reflections) 0.3678, wR_2 (all reflections) 0.5506; goodness of fit indicator 1.001).

FT-IR spectra of free silica **SiG**, $\mathbf{SiNH_2}$, and **SiNPz-Th** are presented in Figure 2. For **SiG**, signals at 3449, 1100, and 970

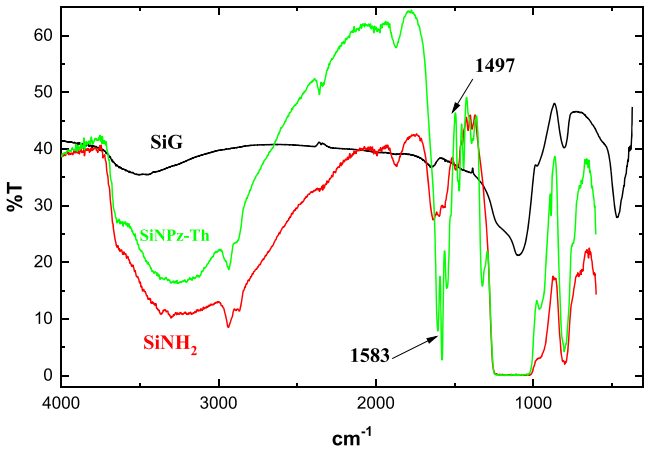


Figure 2. FTIR spectra of the **SiG**, $\mathbf{SiNH_2}$, and **SiNPz-Th**.

cm^{-1} correspond to Si−OH, Si−O−Si, and Si−O, which are characteristic adsorption peaks of silica. For $\mathbf{SiNH_2}$, two adsorption peaks located at 2941 and 1560 cm^{-1} are assigned to CH and NH_2 elongation vibrations, demonstrating the presence of propylamine groups onto the silica surface. The spectrum of **SiNPz-Th** exhibits two new peaks appearing at 1497 and 1583 cm^{-1} which are related to C=C and C=N stretching vibrations, respectively, indicating that $\mathbf{L_1}$ has been immobilized onto the silica surface successfully.

https://dx.doi.org/10.1021/acsomega.0c01616
ACS Omega 2020, 5, 17324−17336

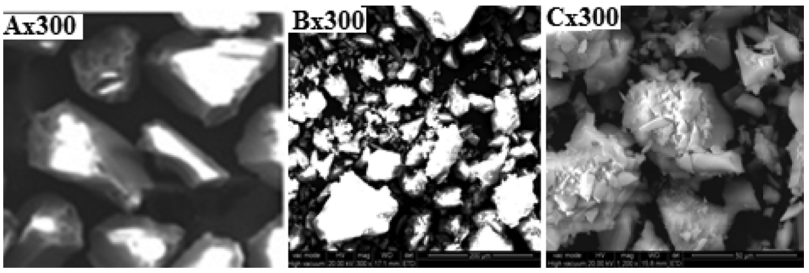


Figure 3. SEM micrographs of **SiG** (A), **SiNH$_2$** (B), and **SiNPz-Th** (C).

Scanning electron microscopy (SEM) images of free silica (**SiG**) and hybrid material (**SiPz-Th**) are presented in Figure 3. It is clear that the surface morphology of **SiNPz-Th** is different from that of **SiG**. The surface of the hybrid material becomes rough, with a wide distribution of micrometer-sized particles. The distinct roughness of the surface indicates successfully functionalized silica with the β-ketoenol-pyrazole-thiophene ligand.

Nitrogen adsorption−desorption isotherms and the corresponding Barrett−Joyner−Halenda (BJH) pore-size distribution of **SiG**, **SiNH$_2$**, and **SiNPz-Th** were examined. The compounds under study exhibit typical IV isotherms with visible hysteresis loops (Figure 4), indicating a mesoporous

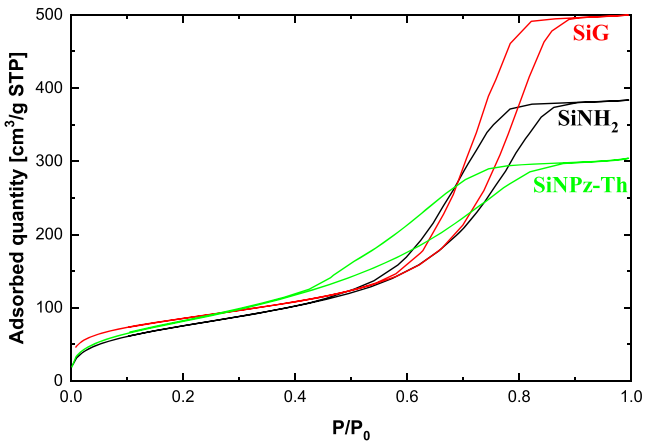


Figure 4. Nitrogen adsorption−desorption isotherm plots of **SiG**, **SiNH$_2$**, and **SiNPz-Th**.

structure.[54] Furthermore, the **SiNPz-Th** displays a Brunauer−Emmett−Teller (BET) surface area, pore volume, and BJH adsorption average pore diameter of 310.11 m^2/g, 0.53 cm^3/g, and 45 Å, respectively, compared to **SiNH$_2$** which shows 283.08 m^2/g BET surface area, 0.69 cm^3/g pore volume, and 88.3 Å BJH adsorption average pore diameter, confirming a marked porosity in the structure. These results indicate the presence of active adsorption sites within the synthesized material.

Thermogravimetric analyses (TGA) were recorded in the temperature ranging from 25 to 800 °C for **SiG**, **SiNH$_2$**, and **SiNPz-Th** (Figure 5). **SiG** presents a weight loss of 3.15% from 25 to 110 °C that corresponds mainly to the loss of water.[55] The second stage of mass loss of 5.85% occurring from 110 to 800 °C is attributed to the condensation of silanol groups.[56] For **SiNH$_2$**, there are two decomposition stages. The first one which starts in the range of 25−100 °C, presenting a mass loss of 1.56% was assigned to the dehydration process.

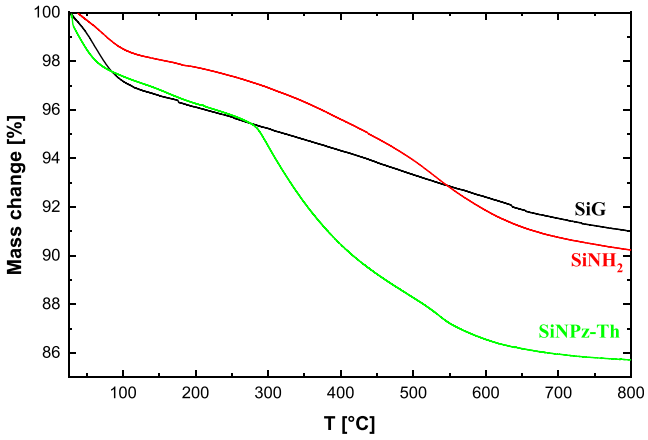


Figure 5. Thermogravimetric profiles of free silica **SiG**, **SiNH$_2$**, and **SiNTh-Th**.

The second one loses 7.22% mass at around 208−800 °C and was ascribed to the decomposition of propylamine immobilized onto silica. **SiNPz-Th** experienced a two-stage weight loss; the first in the range of 25−108 °C for about 2.77% which is due to water release. Ultimately, the highest weight loss of 11.55% occurring over the range 257−800 °C was ascribed to the decomposition of the β-ketoenol-pyrazole-thiophene ligand.

Effect of pH on the Adsorption. The pH of a solution is the key factor that significantly influences adsorption characteristics. The impact of pH on the removal of Pb(II), Cu(II), Zn(II), and Cd(II) by **SiNPz-Th** is depicted in Figure 6. The adsorption capacity of Pb(II), Cu(II), Zn(II), and Cd(II) increased with an initial pH increase. At low pH, the adsorption capacity was fairly low because the functional groups of β-ketoenol-pyrazole-thiophene were protonated due to the presence of excess protons in the solution, which caused decrease in the adsorption capacities of metal ions as a result of the electrostatic repulsion between positive charge of metal ions and that of the protonated ligand. With the increase of pH, the number of H^+ in the solution reduces and the protonation of functional groups decreases, leading to improved active binding sites being available for complexation of metal ions. Hence, the optimum adsorption is achieved at pH = 6. However, when pH is higher than 7, it leads to the precipitation of $M(OH)_2$. This is consistent with the point of zero charge (PZC) which corresponds to the pH at which the surface charge is zero. Indeed, the PZC of initial silica was determined as pH = 2.3 by using a simple described method.[57] Surface coverage of the modified silica with an organic compound leads to an increase of the PZC of the silica surface from pH = 2.3 to pH = 7 due to the basicity of the ligand used.

https://dx.doi.org/10.1021/acsomega.0c01616
ACS Omega 2020, 5, 17324−17336

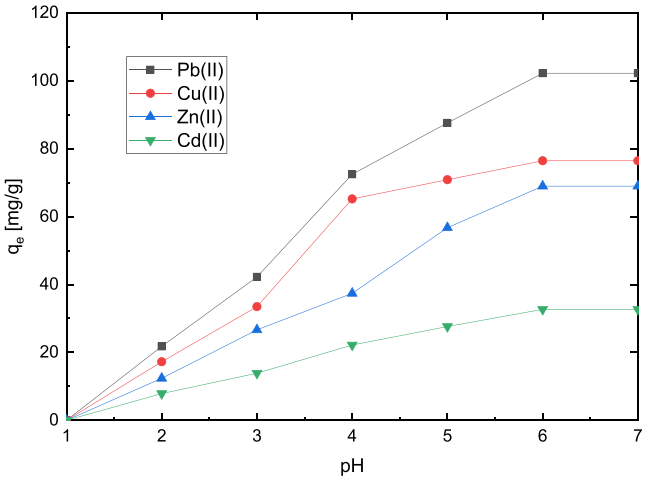


Figure 6. Effect of solution pH on the removal of Pb(II), Cu(II), Zn(II), and Cd(II) by **SiNPz-Th** at optimum concentration (110 mg/L in each case) for 60 min at 25 °C.

At this pH_{PZC}, corresponding to the total deprotonation of the ligand, maximum sorption was observed.

Effect of Contact Time. The contact time is one of the most important factors to consider in the adsorption procedure. In this work, the contact time was evaluated over the range 0−35 min by mixing the adsorbent (10 mg) with 10 mL of solution at pH = 6 and 25 °C. As can be seen from Figure 7, when the contact time increased, the adsorption

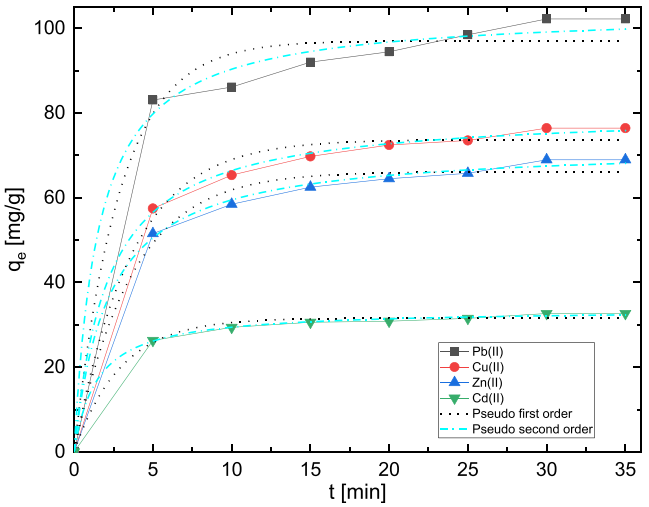


Figure 7. Pseudo-second-order model fit for the adsorption of Pb(II), Cu(II), Zn(II), and Cd(II) by **SiNPz-Th**. Adsorption conditions: V = 10 mL, m = 10 mg of adsorbent, pH = 6, and optimum concentration (110 ppm in each case) at 25 °C.

capacity increased gradually and then remained stable after about 20 min; in the first 5 min, more than 90% of the equilibrium adsorption was attained. These results indicate that the adsorption is very rapid and may mainly be due to the active site receptors which are sufficient to facilitate the quick sorption of Pb(II), Cu(II), Zn(II), and Cd(II) ions.

Kinetic Modeling. Experimental data were described by two kinetic models to explain the mechanism of control of metal-ion adsorption: the pseudo-first-order and pseudo-second-order models.[58,59]

The nonlinear form of the pseudo-first-order kinetic mathematical expression is expressed as follows

$$q_t = q_e[1 - e^{-k_1 t}] \quad (1)$$

where q_e (mg/g) and q_t (mg/g) are the equilibrium adsorption amount and the adsorption capacity over a period of time, and k_1 (min^{-1}) is the rate constant of the first-order-adsorption.

The nonlinear form pseudo-second-order model is given as

$$q_t = \frac{k_2 q_e^{\ 2} t}{1 + k_2 q_e t} \quad (2)$$

where k_2 (g/mg/min) is the pseudo-second-order adsorption rate constant.

The results were illustrated in Figure 7, whereas the fitting parameters of the two models are gathered in Table 1. A fine analysis suggests that the pseudo-second-order model is more suitable for describing the kinetic adsorption process of Pb(II), Cu(II), Zn(II), and Cd(II). Furthermore, the results obtained from this model indicate that a chemisorption mechanism adsorption, involving complexation reaction shared between the adsorbate and adsorbent, is effective.

Effect of Concentration. The concentration effect of the metal ions on adsorption is very important. It can provide basic information about interaction between adsorbate and adsorbent. The initial concentration of all metal ions varies from 10 to 300 mg/L using the batch method. The impact of concentration on adsorption of Pb(II), Cu(II), Zn(II), and Cd(II) on **SiNPz-Th** is displayed in Figure 8. It is clearly shown that the adsorbed quantity of metal ions increases in parallel with the increase in the concentration, which indicates that the adsorption promotes a high concentration which corresponds to a greater mass transfer driving force at a high concentration gradient. It is shown in Figure 8 that the equilibrium adsorption of metal ions on **SiNPz-Th** was in the order of Pb(II) > Cu(II) > Zn(II) > Cd(II).

Adsorption Isotherms. Langmuir and Freundlich models are commonly employed to reveal the isotherm adsorption mechanism[60,61] in various fields. The Langmuir model assumes single molecular layer adsorption with the adsorption sites which are uniformly distributed evenly on the surface of the adsorbent. The nonlinear form of the Langmuir model can be expressed by the following equation

$$q_e = \frac{qK_L C_e}{1 + K_L C_e} \quad (3)$$

where C_e (mg/L) is the equilibrium concentration of the solution; q_e (mg/g) the amount adsorbed at equilibrium; q (mg/g) is the saturated adsorption capacity; and K_L (L/mg) represents the Langmuir constant.

The Freundlich model is employed to describe the adsorption of an adsorbate on non-uniform surfaces with an adsorption multilayer. The Freundlich model is represented by the equation

$$q_e = K_F C_e^{\ 1/n} \quad (4)$$

where q_e (mg/g) represents the equilibrium adsorption capacity; K_F (mg/L) and n are the Freundlich constants; and C_e (mg/L) is the equilibrium concentration of metal ions.

As displayed in Figure 8 and Table 2, the adsorption capacities q calculated using the Langmuir model 103.84 ± 2.44, 85.00 ± 1.07, 77.71 ± 2.28, and 35.91 ± 0.41 of Pb(II),

https://dx.doi.org/10.1021/acsomega.0c01616
ACS Omega 2020, 5, 17324−17336

Table 1. Kinetics Models Data for Metal Removal onto SiNPz-Th

	Pb(II)	Cu(II)	Zn(II)	Cd(II)
q_{exp} (mg/g)	102.20	76.42	68.95	32.68
		Pseudo-First-Order		
q_e (mg/g)	97.02 ± 2.23	73.73 ± 1.23	66.16 ± 1.21	31.58 ± 0.40
K_1 (min^{-1})	0.34 ± 0.06	0.27 ± 0.02	0.27 ± 0.03	0.33 ± 0.03
R^2	0.8	0.99	0.98	0.99
		Pseudo-Second-Order		
q_e (mg/g)	104.16 ± 2.35	80.44 ± 0.76	72.31 ± 0.89	33.67 ± 0.28
K_2 (g/mg/min)	0.006 ± 0.001	0.005 ± 4.69 × 10^{-4}	0.006 ± 6.55 × 10^{-4}	0.02 ± 0.001
R^2	0.99	0.99	0.99	0.99

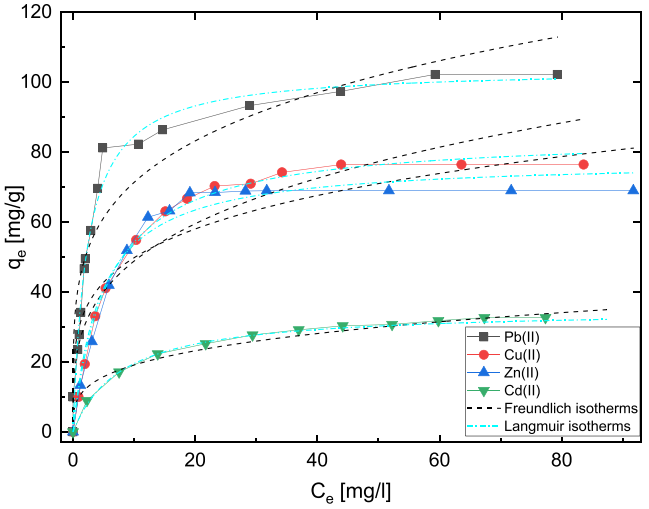


Figure 8. Langmuir and Freundlich adsorption model fits for Pb(II), Cu(II), Zn(II), and Cd(II) by **SiNPz-Th**. Adsorption conditions: 10 mg, V = 10 mL, 25 °C, and pH = 6 for Pb(II), Zn(II), Cu(II), and Cd(II) ions.

Cu(II), Zn(II), and Cd(II), respectively, are close to the experimental data. As a result, the Langmuir model gave better fitting of Pb(II), Cu(II), Zn(II), and Cd(II) adsorption on **SiNPz-Th** compared to the Freundlich model, thus suggesting that the adsorption of metal ions corresponds to a one-layer adsorption process on the **SiNPz-Th** surface.

Adsorption Thermodynamics. To examine the impact of temperature on the adsorption efficiency of the **SiNPz-Th** adsorbent, Gibbs free energy ($\Delta G°$), enthalpy change ($\Delta H°$), and entropy change ($\Delta S°$) can be calculated by the following equations[62]

$$K_d = \frac{C_0 - C_e}{C_e} \quad (5)$$

$$K_c = K_d \times 1000 \times M \quad (6)$$

$$\Delta G° = -RT \ln K_c \quad (7)$$

$$\ln K_c = -\frac{\Delta H°}{RT} + \frac{\Delta S°}{R} \quad (8)$$

where R (8.314 J/mol/K) is the gas constant, M (g/mol) is the molar mass, T (K) is the temperature, K_d is the distribution coefficient, K_c is the equilibrium constant, C_0 (mg/L) is the initial concentration of metal ion, and C_e (mg/L) is the equilibrium concentration of metal ion.

The results are given in Figure 9 and in Table 3. The positive $\Delta H°$ value indicates the endothermic process of the

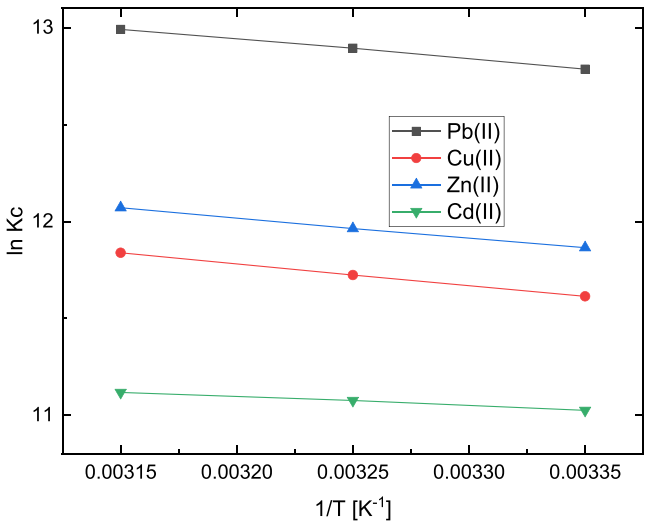


Figure 9. Effect of temperature on the adsorption of metal ions onto **SiNPz-Th**.

Table 2. Adsorption Isotherm Parameters for the Removal of Heavy Metals onto SiNPz-Th

	Pb(II)	Cu(II)	Zn(II)	Cd(II)
q_{exp} (mg/g)	102.20	76.42	68.95	32.68
		Freundlich Isotherm Model		
n	4.51 ± 0.57	3.50 ± 0.49	4.53 ± 0.94	3.39 ± 0.29
K_F (mg/L)	42.82 ± 3.82	25.33 ± 3.56	29.98 ± 4.741	9.66 ± 0.91
R^2	0.90	0.90	0.84	0.97
		Langmuir Isotherm Model		
K_L (L/mg)	0.437 ± 0.04	0.17664 ± 0.00943	0.22207 ± 0.03091	0.12128 ± 0.00654
q (mg/g)	103.84 ± 2.44	85.00 ± 1.07	77.71 ± 2.28	35.91 ± 0.41
R^2	0.98	0.99	0.97	0.99

https://dx.doi.org/10.1021/acsomega.0c01616
ACS Omega 2020, 5, 17324−17336

Table 3. Adsorption Models Used in This Work and Their Associated Parameters

metal	$\Delta H°$ (kJ/mol)	$\Delta S°$ (J/K/mol)	T (K)	$\Delta G°$ (kJ/mol)
Pb(II)	08.16	133.59	299.15	−31.80
			309.15	−33.14
			319.15	−34.47
Cu(II)	08.93	126.38	299.15	−28.88
			309.15	−30.13
			319.15	−31.41
Zn(II)	08.31	125.99	299.15	−29.50
			309.15	−30.74
			319.15	−32.02
Cd (II)	03.67	103.96	299.15	−27.42
			309.15	−28.46
			319.15	−29.49

adsorption. The positive $\Delta S°$ value reveals that entropy increases during the adsorption. The removal of Pb(II), Cu(II), Zn(II), and Cd(II) by **SiNPz-Th** is a spontaneous process according to the negative value of $\Delta G°$.

Adsorption Mechanism. DFT, NCI, and QTAIM calculations were applied to understand the adsorption selectivity and adsorption behavior difference between Pb(II), Cu(II), Zn(II), and Cd(II) in the presence of our hybrid material. Topology analysis of electron density in QTAIM was used to describe the electron density population for each atomic space of **SiNPz-Th** based on the delocalized and localized index measurements of electron density which is shared or exchanged between two atoms; the isosurface map of the dispersed electron density was also output. The uncommitted electron population (UEP), for example, the non-bonding region, is related to the atomic centers of **SiNPz-Th** that should be coordinated with an empty d orbital of the metal ion. Thus, it can be used as information to find the possible active sites of **SiNPz-Th** that can interact with a 3d metal ion, even if we do not pretend to fully describe the complexation which could involve solvent species. The Lewis structure, the UEP of the significant atoms, and the shape of electron density of the entire **SiNPz-Th** are displayed in Figure 10. From Figure 10, we note that the most preferred active interaction sites of **SiNPz-Th** are the oxygen atom (O34) of the hydroxyl group and the nitrogen atom (N18) of the imine function because their UEP are significant enough (>2.2 e) to establish orbital bonds with the metal ion. The situation differs for the two heteroatoms, such as sulfur S37 of the thiophene group and nitrogen N10 of the pyrazole, their UEP being not sufficient to create a novel orbital bond with the vacant d orbital (<1.3 e). In other words, despite the nitrogen atom N4 displaying an important UEP value (>3 e), a part of it should be delocalized in the pyrazole ring and continually this UEP will be renewed by its electro-donating methyl group substituent (Figure 10a). These findings were reinforced using one of the most conceptual DFT indices, namely the nucleophilic Parr functions (P^-)[63] which is a powerful approach to evaluate the electron-donating ability of compound sites. These functions are obtained from the analysis of the Mulliken atomic spin density at the radical cation by removing an electron. These functions evidence again the most nucleophilic sites of **SiNPz-Th** which can interact with a metal ion (Figure 10b, right). It should be noted that a negative value of P^- corresponds to a non-reactive site and consequently the most nucleophilic sites will correspond to the highest values of P^-.

The NCI theory has been commonly used to characterize three types of inter/intramolecular interactions: strong attractive interactions (in blue), weak interactions (in green),

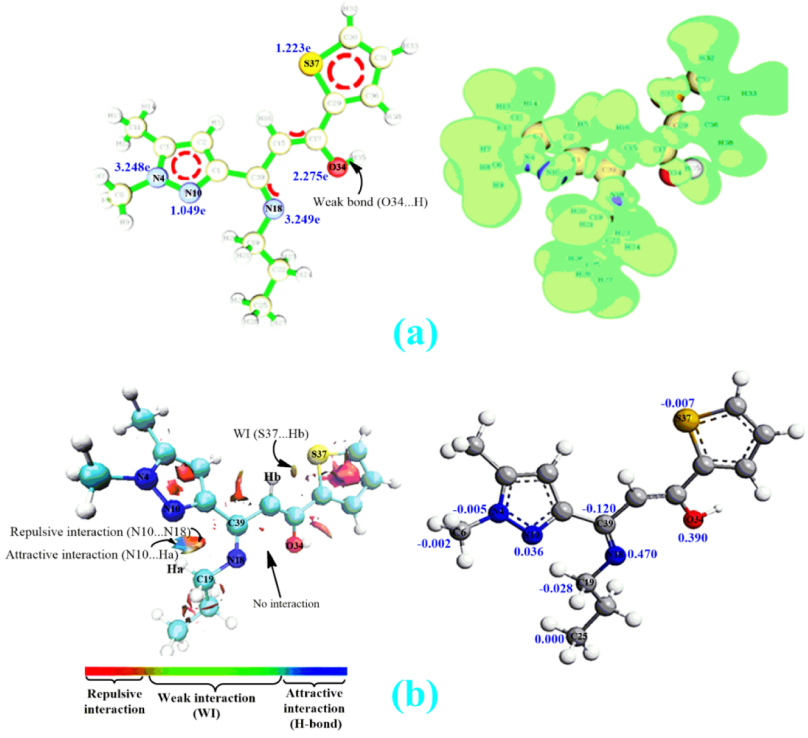


Figure 10. (a) (left) Schematic view of Lewis structure and significant values of UEP; (right) shape of electron density of the entire **SiNPz-Th**. (b) (left) NCI isosurface; (right) nucleophilic P—Parr functions of **SiNPz-Th**.

https://dx.doi.org/10.1021/acsomega.0c01616
ACS Omega 2020, 5, 17324−17336

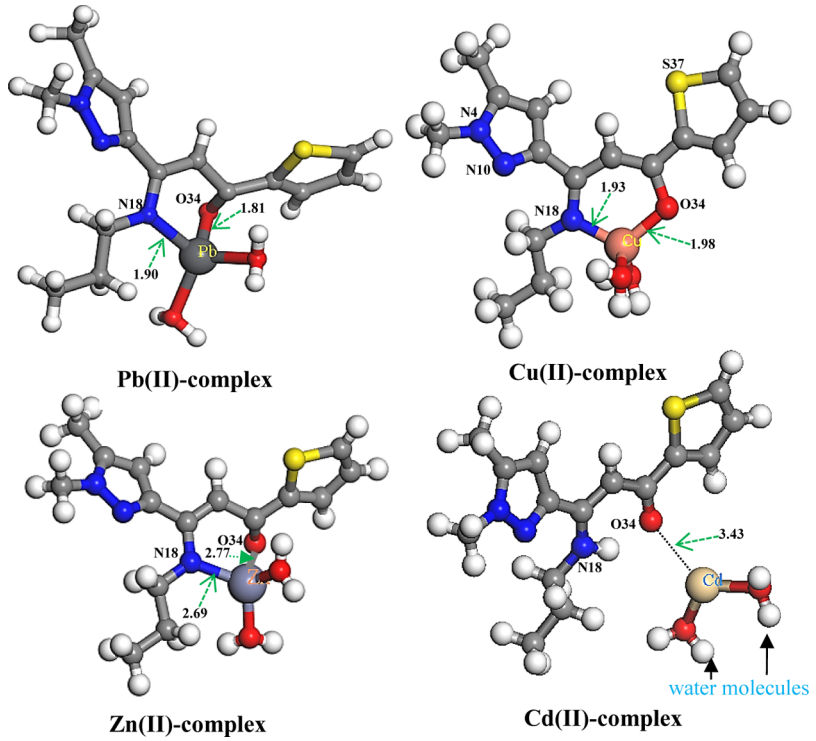


Figure 11. Optimized geometry of complexes formed between reactive atoms of the ligand/water and metal ions (water(2)···M(II)···ligand).

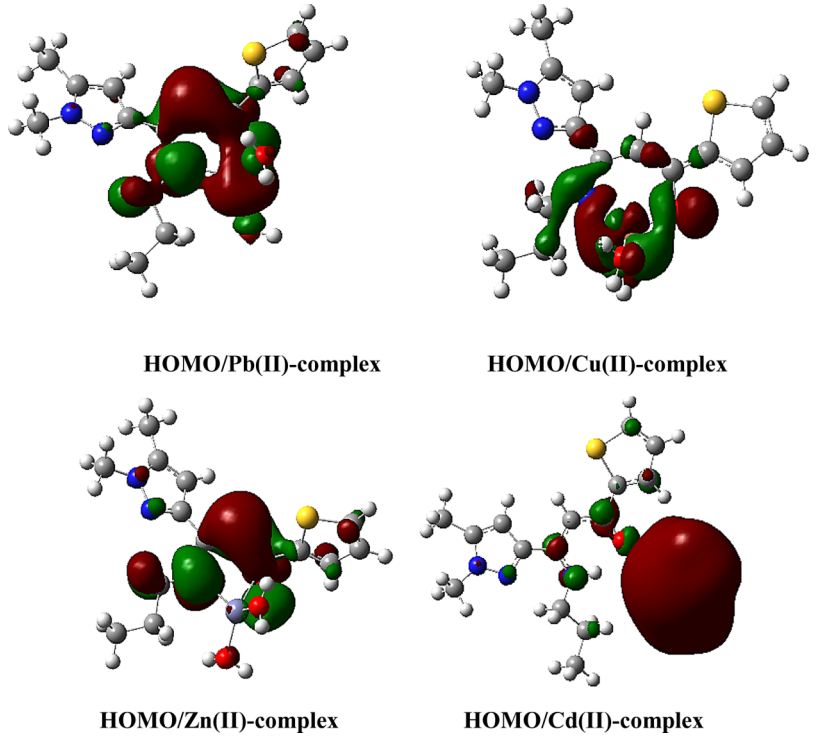


Figure 12. Plot of HOMO for our M(II) complexes.

and repulsive interactions (in red) as represented in Figure 10b (left). On one hand, both repulsive and attractive interactions are found between the two nitrogen atoms (N10···N18) and between hydrogen H_a and nitrogen N10 atoms (Ha···N10), respectively. On the other hand, a weak interaction exists between the thiophene sulfur atom S37 and hydrogen atom H_b (S37···H_b). In contrast, no interactions were found between the hydroxyl oxygen atom O34 and the imine nitrogen atom N18, which supports the results obtained from DFT and QTAIM analysis, which suggested that these two atoms are responsible for the binding ability of **SiNPz-Th** to the metal ion.

Based on these computations, the possible optimized structures of mononuclear coordination complexes of M(II)

https://dx.doi.org/10.1021/acsomega.0c01616
ACS Omega 2020, 5, 17324−17336

Table 4. NBO Analysis Calculations for the M(II) Complex (M: Pb, Cu, Zn and Cd)

		$E^{(2)}$ energy (kcal/mol)	
	EC of M, O34 and N18	LP(N18) → LP*(M)	LP(O34) → LP*(M)
Pb(II) complex	Pb:[core]$6s^{1.83}6p^{1.20}$	88.33	25.54
	O34:[core]$2s^{0.21}2p^{1.11}3p^{0.00}$		
	N18:[core]$2s^{0.24}2p^{1.71}3p^{0.00}$		
Cu(II) complex	Cu:[core]$4s^{0.17}3d^{4.93}4p^{0.06}$	53.24	13.23
	O34:[core]$2s^{0.84}2p^{2.58}3p^{0.01}$		
	N18:[core]$2s^{0.68}2p^{2.10}3p^{0.01}$		
Zn(II) complex	Zn:[core]$4s^{1.96}3d^{9.99}4p^{0.07}$	35.64	10.68
	O34:[core]$2s^{1.58}2p^{5.01}3p^{0.01}$		
	N18:[core]$2s^{1.41}2p^{5.09}3p^{0.01}$		
Cd(II) complex	Cd:[core]$5s^{1.98}4d^{10.00}5p^{0.03}$		4.32
	O34:[core]$2s^{1.74}2p^{5.12}3p^{0.01}$		
	N18:[core]$2s^{1.47}2p^{4.31}3p^{0.01}$		

(M = Pb, Cu, Zn, and Cd) with **SiNPz-Th** are presented in Figure 11. In brief, **SiNPz-Th** coordinates with Pb(II), Cu(II), and Zn(II) using an oxygen atom O34 and a nitrogen atom N18 to form stable complexes, whereas Cd(II) is only bonded by an oxygen atom O34 (Figure 11). Thus, **SiNPz-Th** adopts a bidentate coordination mode for Pb(II), Cu(II), and Zn(II) ions, whereas a monodentate mode if found for Cd(II) ion. Interestingly, we note that when Cd(II) interacts with the oxygen atom O34 of **SiNPz-Th**, the hydrogen atom of the hydroxyl group (−OH) is easily captured by the nitrogen atom N18; and thus weakens the coordination of Cd(II) with the ligand. Thus, coordination is weaker for Cd(II) compared to other metal ions, a situation confirmed by experimental results which show the weakest adsorption for Cd(II) ions.

Figure 12 displays the isodensity surface plots of the highest occupied molecular orbital (HOMO) analysis. This calculation reflects also the chemical reactivity related to the lone paired electron transport from the ligand to the empty d orbital of the metal ion. As shown in Figure 12, the HOMO is not localized at the pyrazole and thiophene rings, which suggests that the nitrogen atoms of pyrazole and sulfur atom thiophene are not reactive toward the metal ion. In other words, the electron density of HOMO for Pb(II), Cu(II), and Zn(II) complexes are mainly located on the oxygen atom O34, nitrogen atom N18, and the adjacent carbon atoms. Whereas, for the Cd(II) complex, the HOMO is nearly spread at the oxygen atoms of complexed water and not over O34 and N18 atoms of the ligand. This situation means that the coordination with Cd(II) is commonly generated from the water molecules and not from the ligand. In other words, the degree associated to the contribution of HOMO for the concerned complexes (Figure 11) can be classified as follow: Pb(II)-complex > Cu(II)-complex > Zn(II)-complex > Cd(II)-complex. This could be a good indication for the coordination selectivity of the metal ion toward the studied ligand. This selectivity will be confirmed in the next part in terms of the natural bond orbitals analysis.

As follows, a natural bond orbital (NBO) analysis[64] for the studied coordination complexes has been undertaken to inspect selectivity of adsorption for Pb(II), Cu(II), Zn(II), and Cd(II); hence, strengths of the studied interactions N18 → M(II) and O34 → M(II) have been further evaluated from second-order stabilization energy $E^{(2)}$ and the electronic configurations (EC) of M(II), O34, and N18. As a large value of $E^{(2)}$ means a more intensive donor−acceptor interaction, these are considered as a good representation of the bond strength. The NBO analysis calculations, listed in Table 4, indicate that the valence ECs of O34 and N18 which are associated to the formed complexes (Figure 11) are ranged as follows: EC(Cd(II)) < EC(Zn(II)) < EC(Cu(II)) < EC(Pb(II)). This supports that the charge transfer of adsorption takes place from O34 and N18 to the empty orbitals of Pb(II), Cu(II), and Zn(II), whereas for the Cd(II) complex, the charge transfer proceeds from O34 and N18 to the empty orbitals of both Cd(II) and the transferred hydrogen atom of hydroxyl group of the ligand, respectively. The calculated stabilization energies $E^{(2)}$ associated to the studied interactions are listed in Table 4.

These results show that the interaction strength ligand → M(II) follows the tendency: Pb(II) > Cu(II) > Zn(II) > Cd(II). To this end, we note that the experimental selectivity (Figure 13) is completely reproduced by the present computational study.[65−73]

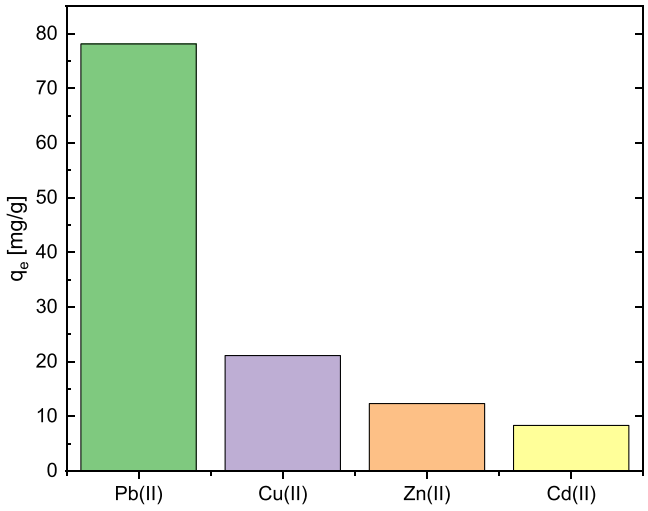


Figure 13. Selectivity of **SiNPz-Th** for Pb(II) removal with initial concentration of 150 mg/L for metal ions.

Adsorption Selectivity of SiNPz-Th. Competitive adsorption of heavy-metal ions on **SiNPz-Th** was investigated using quaternary mixed solutions (Pb(II), Cu(II), Zn(II), and Cd(II)) using the batch method under optimum conditions (Figure 13). The **SiNPz-Th** material presents a higher selectivity toward Pb(II) ions compared to other common divalent ions such as Cu(II), Zn(II), and Cd(II) ions. The high

https://dx.doi.org/10.1021/acsomega.0c01616
ACS Omega 2020, 5, 17324−17336

selectivity of **SiNPz-Th** for Pb(II) should be ascribed to the β-ketoenol-pyrazole-thiophene functional groups bonded onto the silica surface, which can coordinate with Pb(II) to form more stable complexes. The reason of the high selectivity adsorption of Pb(II) maybe due to the large ionic radius and the electronegativity of lead. It is clear that the **SiNPz-Th** is capable of selectively adsorbing Pb(II) ions from the mixture of several metal ions in wastewater.

Effect of Electrolyte. In the actual environmental pollution, there are a variety of foreign ions, which can reduce the adsorption efficiency. It is therefore essential to investigate the impact of existing ions in the solution onto the sorption of Pb(II) ions. The experiment of Pb(II) sorption was thus performed in the presence of four co-existing ions (K^+, Na^+, Ca^{2+}, and Mg^{2+}) examined under optimum conditions. Table 5

Table 5. Effect of Interfering Ions on the Recovery of Pb(II) Ions Adsorbed on the SiNPz-Th Sorbent (Concentration of Pb(II) Ion is 0.05 μg/mL)

interfering ion	concentration (μg/mL)	recovery of Pb(II) (%)
K^+	3000	97.69
Na^+	3000	99.15
Ca^{2+}	2000	96.32
Mg^{2+}	2000	95.12

represents the effect of adsorption capacity of Pb(II) (C_0 = 0.05 μg/mL) onto **SiNPz-Th** in the presence of co-existing ions. It is clear that the adsorption efficiency was maintained more than 98%, thus suggesting that the adsorption of Pb(II) ions is not weakened by the presence of co-existing ions. This experimental study of co-existing ions confirms that the adsorbent **SiNPz-Th** presents higher adsorption capacity toward Pb(II) and can potentially be applied to a real sample that contains various ions.

Desorption and Recycling. Reusability is one of the crucial indicators for assessing whether an adsorbent is practicable or not. Desorption of the adsorbent was examined by adding 2 mol/L HCl to 10 mg of **SiNPz-Th** after having absorbed Pb(II). The suspension was stirred for 60 min. Then, the **SiNPz-Th** was neutralized by a NaOH solution and dried in vacuum for the next adsorption. Table 6 represents the

Table 6. Adsorption/Regeneration of Hybrid Material Toward Pb(II)

cycle number	Pb(II)(mg/g)
1	102.27
2	102.19
3	101.21
4	100.49
5	100.07

removal efficiency of **SiNPz-Th** after five cycles for Pb(II) ions. Interestingly, the adsorbent retained more than 96% of their adsorption capacity. Thus, **SiNPz-Th** presents outstanding recyclability and applicability which could be useful for the purification of lead contaminated water or the handling of wastewater.

Adsorption of Pb(II) from Real Water Samples. The feasibility of **SiNPz-Th** for elimination of Pb(II) ions from field water samples was tested by mixing 10 mg of the adsorbent for 10 mL of water followed by the addition of 0.5 mL of HNO_3 at 25 °C. The choice was focused on two types of river water samples selected from the Oriental Morocco area: (i) Ghiss river (located next to Al Hoceima) where pH = 7.7, total dissolved solids (TDS) = 1297 mg/L, and conductivity (σ) = 1733 μS/cm. (ii) Toussit-Bou-Beker river (in the Jerada-Oujda region) where pH = 7.1, TDS = 2031 mg/L, and σ = 2301 μS/cm. The water samples were filtered with a 0.45 μm nylon membrane to remove large particle-size impurities. As the designated real water samples did not enclose any Pb(II) ions, which is the metal ion for which our **SiNPz-Th** adsorbent would be the most efficient, the samples had to be doped with Pb(II) ions. The choice was made on 5 and 10 mg/L of Pb(II). Clearly, the removal efficiency of Pb(II) ions was high up to 96% (Table 7). This result clearly

Table 7. Analysis of Pb(II) in Real Water Samples

water samples	added Pb(II) (mg/L)	removal efficiency (%)
Touissit-Bou-Beker water	5	96.34
	10	94.67
Ghiss water	5	96.65
	10	95.98

indicates that our developed **SiNPz-Th** adsorbent is more effective in purification of real water and could be used as an excellent candidate in water pollution treatment.

Comparison with Other Adsorbents. A comparison of the Pb(II) adsorption performance of **SiNPz-Th** with other adsorbents reported is useful to place our hybrid material's properties in perspective (Table 8). Indeed, the **SiNPz-Th**

Table 8. Comparison of the Maximum Adsorption Capacities of Pb(II) by Different Adsorbents Reported in the Literature

support: silica gel/ligand	references	metal ion (mg/g)
SiNPz-Th	this work	**102.27**
free silica (**SiG**)		04.32
propylamine (**$SiNH_2$**)		06.33
porphyrin	38	55.17
bispyrazole	39	35.26
TOES	65	75.60
dithiocarbamate	66	42.19
2-hydroxy-3-methoxy benzaldehyde	67	02.27
3-(2-aminoethylamino)propyl	68	19.61
3-mercaptopropyl	69	32.58
PMAEEDA	70	61.90
commercial activated carbon (CS-1501)	71	25.90
commercial activated carbon (RS-1301)	71	35.43
commercial activated carbon (NC-60)	71	25.30
commercial activated carbon (aktivkohle)	72	23.42
biochar	73	37.82

adsorbent shows greater maximum adsorption capacity for Pb(II) ions (102 mg/g) compared to the previous silica hybrids; it is also higher when comparison is made with known commercialized activated carbons. This clearly indicates that the **SiNPz-Th** adsorbent could be considered as a useful solution in Pb(II) remediation applications.

CONCLUSIONS

A new sustainable and environmentally friendly hybrid inorganic−organic adsorbent including a novel β-ketoenol-

https://dx.doi.org/10.1021/acsomega.0c01616
ACS Omega 2020, 5, 17324−17336

pyrazole-thiophene receptor has been prepared and used for the removal of heavy-metal ions (Pb(II), Cu(II), Zn(II), and Cd(II)) from water samples. Superior characteristics were observed for Pb(II) ions with an adsorption capacity not less than 102.20 mg/g at 30 min and pH = 6, coupled to an excellent recyclability up to minimum five cycles. The adsorbent obtained has extremely high adsorption capacity and selectivity of Pb(II) from water. Insights to the adsorption and selectivity mechanism were gained by a computational study which supported metal-ion coordination following a bidentate mode for Pb(II), Cu(II), and Zn(II) and a monodentate mode for Cd(II). In addition, the affinity of our hybrid material toward Pb(II) was confirmed by our computational study. All these results highlight that our hybrid material has a good potential to be an advanced adsorbent for lead ion removal in aquatic media.

EXPERIMENTAL SECTION

Materials and Methods. All reagents (Aldrich, purity 99.5%) were of analytical grade. Initial silica gel (60 Å, 70−230 mesh) (E. Merck) was activated at 120 °C for 24 h. The quantification of metal ions in aqueous solutions was determined by atomic absorption (Spectra Varian A.A. 400 spectrophotometer). The surfaces were characterized by a CHN analyzer (Microanalysis Center Service, CNRS), Fourier-transform infrared spectroscopy (FTIR, Perkin Elmer System 2000), SEM (FEI-Quanta 200), TGA (Perkin Elmer Diamond), ^{13}C solid state nuclear magnetic resonance (NMR, CP MAX CXP 300 MHz), and BET (ThermoQuest Sorpsomatic 1990 analyzer).

Preparation of (*Z*)-1-(1,5-Dimethyl-1*H*-pyrazol-3-yl)-3-hydroxy-3-(thiophen-2-yl)Prop-2-en-1-one (L_1). Ethyl 1,5-dimethyl-1*H*-pyrazole-3-carboxylate (2 g, 11.89 mmol) was dissolved in toluene (25 mL). Metallic sodium (0.4 g, 17.39 mmol) was added to this solution with stirring; then, a solution of 2-acetylthiopene (1.5 g, 11.89 mmol) in toluene (3.5 mL) was slowly added at 0 °C; the reaction mixture was kept under stirring for about 3 days at 25 °C. The mixture was filtered, the residue was washed in toluene (15 mL), dissolved in water (10 mL), and treated with acetic acid (1 mL) to pH = 5. The product obtained was removed with CH_2Cl_2 (3 × 5 mL). The resulting product was recrystallized from methanol (1 mL) leading to single crystals suitable for X-ray diffraction analysis. Yield: 0.89 g, 30%; mp (hot MeOH) = 110 °C; R_f 0.42 (CH_2Cl_2/MeOH 9:1) silica; FTIR (KBr, cm^{-1}) ν(OH): 3434; ν(C═O): 1672; ν(C═C enolic): 1531; ^1H NMR (DMSO, δ (ppm)): 2.30 (s, 3H, Pz-CH_3); 3.84 (s, 3H, CH_3−N); 4.56 (s, 0.1H, keto, CH_2); 6.58 (s, 1H, Pz−H); 6.80 (s, 0.9H, enol, C−H); 7.13 (m, 1H, Th-Hβ); 7.60 (d, 1H, Th-Hγ); and 7.79 (d, 1H, Th-Hα). ^{13}C NMR (DMSO, δ (ppm)): 11.41 (1C, Pz-CH_3); 37.00 (1C, CH_3−N); 46.76 (1C, keto CH_2); 92.89 (1C, enol C−H); 106.11 (1C, CH-Pz); 128.32 (1C, Th-Hγ); 130.20 (1C, Th-Cβ); 132.16 (1C, Th-Cα); 140.46 (1C, Th-Cε); 177.87 (1C, C−OH); and 180.96 (1C, C═O). *m*/*z*: (M + H)$^+$ 249. Anal. Calcd for $C_{12}H_{12}N_2O_2S$: C, 58.05; H, 4.87; N, 11.28. Found: C, 58.02; H, 4.99; N, 11.31.

Preparation of Amine-Functionalized Silica ($SiNH_2$). Amine-functionalized silica **$SiNH_2$** was constructed following a similar procedure reported earlier.[31,32] A suspension of activated silica gel (30 g) and 10 mL of 3-aminopropyltrimethoxysilane were fully mixed in 200 mL dry toluene in the presence of N_2. Then, the reaction mixture was refluxed for 24 h, the material **$SiNH_2$** was obtained after filtration and Soxhlet extraction by anhydrous methanol for 12 h, and finally dried under vacuum at 60 °C for 24 h.

Fabrication of the SiNPz-Th Adsorbent. A mixture of L_1 (4 g) and **$SiNH_2$** (5 g) in methanol (30 mL) was stirred, refluxed for 12 h. Then, the solid was obtained after separation and Soxhlet extraction with the solvent mixture MeOH/CH_2Cl_2 for 12 h. Finally, the obtained modified silica was dried in an oven at 60 °C for 24 h.

Batch Adsorption Experiments. For studying the adsorption properties of **SiNPz-Th**, the batch experiment was evaluated following the impact of the pH, initial concentrations, contact time, and adsorption temperature. The adsorption experiment of **SiNPz-Th** toward Pb(II), Cu(II), Zn(II), and Cd(II) was investigated by stirring 10 mg of the adsorbent with 10 mL of a metal salt solution ($Pb(NO_3)_2{\cdot}6H_2O$, $Cu(NO_3)_2{\cdot}3H_2O$, $Zn(NO_3)_2{\cdot}6H_2O$, and $Cd(NO_3)_2{\cdot}6H_2O$) in 50 mL tubes at room temperature. The pH values of Pb(II), Cu(II), Zn(II), and Cd(II) solutions were adjusted from 1 to 7 using dilute HCl or NaOH solutions. Meanwhile, the adsorption isotherm experiments were studied with initial concentrations ranging from 10 to 300 mg/L for all metal ions with pH = 6 at 25 °C for 60 min. The effect of contact time was studied from 5 to 60 min at 25 °C. The adsorption thermodynamics were investigated at different temperatures (25, 35, and 45 °C) for 60 min. After that, the concentration of each metal ion was determined by atomic adsorption measurements, and the adsorption capacity was calculated according to the following equation.[74]

$$q_e = (C_0 - C_e) \times V/W \tag{9}$$

where q_e (mg/g) is the adsorption amount, C_0 (mg/L) is the initial concentration, C_e (mg/L) is final equilibrium concentrations, V (L) is the volume of the solution, and W (g) represents the weight of adsorbent.

Computational Methods. The selectivity and mechanism of metal adsorption were further supported by DFT,[75] QTAIM,[76] and NCI[77] analysis using GAUSSIAN 09[78] and Multiwfn[79] software. Optimization of the studied entities such as the ligand, metal ions M(II) (Pb(II), Cu(II), Zn(II) and Cd(II)), and M(II)-complexes were performed using DFT based on Beck's three parameter exchange functional and Lee−Yang−Parr nonlocal correlation functional (B3LYP),[80] combined to the 6-311G++(d,p) basis set,[81] for carbon, hydrogen, nitrogen, sulfur, and nitrogen atoms and to the basis LANL2DZ level[82] for the metal. The intramolecular interactions of **SiPz-Th** were evaluated in terms of NCI analysis. This approach is based on the relationship between the electron density $\rho(r)$ and the reduced density gradient s and is given as follows

$$s = \frac{1}{2(3\pi^2)^{1/3}} \frac{|\nabla \rho|}{\rho^{4/3}} \tag{10}$$

It allows to give isosurfaces of s at low densities and thus to visualize the position and nature of noncovalent interactions in the 3D space (whichever repulsive, van der Waals, attractive, or all). This method has also been recently used to afford a more comprehensive understanding of noncovalent bonding. Furthermore, the strength of bonding interactions has been estimated based on the second-order stabilization energy $E^{(2)}$ calculations,[83,84] which are related in this work to the delocalization of lone pair orbitals (LP) of **SiNPz-Th** to antibonding orbitals (LP*) of metal ions.

https://dx.doi.org/10.1021/acsomega.0c01616
ACS Omega 2020, 5, 17324−17336

Single Crystal X-ray Crystallography. Single-crystal X-ray diffraction data for $\mathbf{L_1}$ were collected on a Rigaku Rapid Axis II-IP-plate, 5 kV, curved detector diffractometer with Mo Kα (λ = 0.71075 Å) radiation. The crystal structure was solved by direct methods,[85] expanded using Fourier techniques and refined by the full-matrix least-squares technique [least squares function minimized: (SHELXL97) $w(F_o^2 - F_c^2)^2$ where w = least squares weights] on F^2 using the SHELXL package.[86] All non-hydrogen atoms were refined anisotropically. Hydrogen atoms were refined using the riding model. All calculations were performed using the Crystal Structure crystallographic software package,[87] except for refinement, which was performed using the SHELXL program. Crystallographic data for the structure reported in this paper was deposited in the Cambridge Crystallographic Data Center with CCDC reference number 1984476. Identical results were obtained on a XtaLAB Synergy-Rigaku Oxford-4 circle diffractometer. The structure was measured and solved using CrysAlisPro software.

■ ASSOCIATED CONTENT

Supporting Information

The Supporting Information is available free of charge at https://pubs.acs.org/doi/10.1021/acsomega.0c01616.

Crystallographic data for the structure reported (CIF)

■ AUTHOR INFORMATION

Corresponding Authors

Said Tighadouini − *Laboratoire de Synthèse Organique, Extraction et Valorisation, Faculté des Sciences Ain-Chock, Université Hassan II Casablanca, Casablanca 20100, Maroc*; Email: tighadouinis@gmail.com

Smaail Radi − *Laboratoire de Chimie Appliquée et Environnement (LCAE), Faculté des Sciences and Centre de l'Oriental des Sciences et Technologies de l'Eau (COSTE), Université Mohamed Premier, Oujda 60000, Morocco*; Email: s.radi@ump.ac.ma

Yann Garcia − *Institute of Condensed Matter and Nanosciences, Molecular Chemistry, Materials and Catalysis Division (IMCN/MOST), Université Catholique de Louvain, Louvain-la-Neuve 1348, Belgium*; orcid.org/0000-0002-3105-0735; Email: yann.garcia@uclouvain.be

Authors

Mohamed El Massaoudi − *Laboratoire de Chimie Appliquée et Environnement (LCAE), Faculté des Sciences, Université Mohamed Premier, Oujda 60000, Morocco*

Zouhair Lakbaibi − *Laboratory of Natural Substances & Synthesis and Molecular Dynamics, Department of Chemistry, Faculty of Sciences and Techniques Errachidia, My Ismail University, Errachidia 52000, Morocco*

Marilena Ferbinteanu − *Faculty of Chemistry, Inorganic Chemistry Department, University of Bucharest, Bucharest 020462, Romania*

Complete contact information is available at: https://pubs.acs.org/10.1021/acsomega.0c01616

Notes

The authors declare no competing financial interest.

■ ACKNOWLEDGMENTS

This work was supported by a bilateral WBI action with Morocco (COP 22 Program 2018−2022), the Fonds De La Recherche Scientifique—FNRS (CDR 33694457) and PPR-P10 CNRST project (Morocco). Appreciation is also extended to the Moroccan Association of theoretical chemists (AMCT) for access to the computational facility.

■ REFERENCES

(1) Ma, L.; Wang, Q.; Islam, S. M.; Liu, Y.; Ma, S.; Kanatzidis, M. G. Highly selective and efficient removal of heavy metals by layered double hydroxide intercalated with the MoS_4^{2-}ion. *J. Am. Chem. Soc.* **2016**, *138*, 2858−2866.

(2) Ling, L.-L.; Liu, W.-J.; Zhang, S.; Jiang, H. Magnesium oxide embedded nitrogen self-doped biochar composites: fast and high efficiency adsorption of heavy metals in an aqueous solution. *Environ. Sci. Technol.* **2017**, *51*, 10081−10089.

(3) Tchounwou, P. B.; Yedjou, C. G.; Patlolla, A. K.; Sutton, D. J. *Molecular, Clinical and Environmental Toxicology: Volume 3: Environmental Toxicology*; Luch, A., Ed.; Springer: Basel, 2012; Vol. 3, pp 133−164.

(4) Jaishankar, M.; Tseten, T.; Anbalagan, N.; Mathew, B. B.; Beeregowda, K. N. Toxicity. mechanism and health effects of some heavy metals. *Interdiscip. Toxicol.* **2014**, *7*, 60−72.

(5) Shafique, U.; Anwar, J.; Anzano, J. M.; Salman, M. *Hazardous Metals: Sources, Toxicity, and Control*; Nova Science Publisher Inc.: New York, 2011; pp 157−186.

(6) Liang, J.; Li, X.; Yu, Z.; Zeng, G.; Luo, Y.; Jiang, L.; Yang, Z.; Qian, Y.; Wu, H. Amorphous MnO_2 modified biochar derived from aerobically composted swine manure for adsorption of Pb(II) and Cd(II). *ACS Sustainable Chem. Eng.* **2017**, *5*, 5049−5058.

(7) Sorouraddin, S. M.; Farajzadeh, M. A.; Okhravi, T. Cyclohexylamine as extraction solvent and chelating agent in extraction and preconcentration of some heavy metals in aqueous samples based on heat-induced homogeneous liquid-liquid extraction. *Talanta* **2017**, *175*, 359−365.

(8) Tavakoli, O.; Goodarzi, V.; Saeb, M. R.; Mahmoodi, N. M.; Borja, R. Competitive Removal of Heavy Metal Ions from Squid Oil under Isothermal Condition by CR11 Chelate Ion Exchanger. *J. Hazard. Mater.* **2017**, *334*, 256−266.

(9) Yang, R.; Li, Z.; Huang, B.; Luo, N.; Huang, M.; Wen, J.; Zhang, Q.; Zhai, X.; Zeng, G. Effects of Fe (III)-Fulvic Acid on Cu Removal via Adsorption versus Coprecipitation. *Chemosphere* **2018**, *197*, 291−298.

(10) Byun, S.-H.; Chung, J. W.; Kwak, S.-Y. Thermally regenerable multi-functional membrane for heavy-metal detection and removal. *J. Water Process Eng.* **2019**, *29*, 100757.

(11) Bora, A. J.; Dutta, R. K. Removal of metals (Pb, Cd, Cu, Cr, Ni, and Co) from drinking water by oxidation-coagulation-absorption at optimized pH. *J. Water Process Eng.* **2019**, *31*, 100839.

(12) Wang, J.; Liu, M.; Duan, C.; Sun, J.; Xu, Y. Preparation and characterization of cellulose-based adsorbent and its application in heavy metal ions removal. *Carbohydr. Polym.* **2019**, *206*, 837−843.

(13) Zhang, Z.; Nui, Y.; Chen, H.; Yang, Z.; Bai, L.; Xue, Z.; Yang, H. Feasible One-Pot Sequential Synthesis of Aminopyridine Functionalized Magnetic Fe_3O_4 Hybrids for Robust Capture Aqueous Hg(II) and Ag(I). *ACS Sustainable Chem. Eng.* **2017**, *7*, 7324−7337.

(14) Deng, S.; Zhang, G.; Wang, P. Visualized Fibrous Adsorbent Prepared by the Microwave-Assisted Method for Both Detection and Removal of Heavy Metal Ions. *ACS Sustainable Chem. Eng.* **2019**, *7*, 1159−1168.

(15) Rosa, M. A.; Egido, J. A.; Márquez, M. C. Enhanced electrochemical removal of arsenic and heavy metals from mine tailings. *J. Taiwan Inst. Chem. Eng.* **2017**, *78*, 409−415.

(16) Mondal, S.; Chatterjee, S.; Mondal, S.; Bhaumik, A. Thioether-Functionalized Covalent Triazine Nanospheres: A Robust Adsorbent for Mercury Removal. *ACS Sustainable Chem. Eng.* **2019**, *7*, 7353−7361.

(17) Nayab, S.; Baig, H.; Ghaffar, A.; Tuncel, E.; Oluz, Z.; Duran, H.; Yameen, B. Silica Based Inorganic-organic Hybrid Materials for the Adsorptive Removal of Chromium. *RSC Adv.* **2018**, *8*, 23963−23972.
(18) Ramalingam, B.; Parandhaman, T.; Choudhary, P.; Das, S. K. Biomaterial Functionalized Graphene-Magnetite Nanocomposite: A Novel Approach for Simultaneous Removal of Anionic Dyes and Heavy-Metal Ions. *ACS Sustainable Chem. Eng.* **2018**, *6*, 6328−6341.
(19) Feng, G.; Ma, J.; Zhang, X.; Zhang, Q.; Xiao, Y.; Ma, Q.; Wang, S. Magnetic natural composite Fe_3O_4-chitosan@bentonite for removal of heavy metals from acid mine drainage. *J. Colloid Interface Sci.* **2019**, *538*, 132−141.
(20) d'Halluin, M.; Rull-Barrull, J.; Bretel, G.; Labrugère, C.; Le Grognec, E.; Felpin, F.-X. Felpin. Chemically Modified Cellulose Filter Paper for Heavy Metal Remediation in Water. *ACS Sustainable Chem. Eng.* **2017**, *5*, 1965−1973.
(21) Wang, Z.; Tan, K.; Cai, J.; Hou, S.; Wang, Y.; Jiang, P.; Liang, M. Silica oxide encapsulated natural zeolite for high efficiency removal of low concentration heavy metals in water. *Colloids Surf., A* **2019**, *561*, 388−394.
(22) Zhou, T.; Cheng, X.; Pan, Y.; Li, C.; Gong, L.; Zhang, H. Mechanical performance and thermal stability of glass fiber reinforced silica aerogel composites based on co-precursor method by freeze drying. *Appl. Surf. Sci.* **2018**, *437*, 321−328.
(23) Bonab, S. A.; Moghaddas, J.; Rezaei, M. In-situ synthesis of silica aerogel/polyurethane inorganic-organic hybrid nanocomposite foams: Characterization, cell microstructure and mechanical properties. *Polymer* **2019**, *172*, 27−40.
(24) Pawlaczyk, M.; Schroeder, G. Adsorption studies of Cu(II) ions on dendrimer-grafted silica-based materials. *J. Mol. Liq.* **2019**, *281*, 176−185.
(25) Soltani, R.; Marjani, A.; Shirazian, S. Facile one-pot synthesis of thiol-functionalized mesoporous silica submicrospheres for Tl(I) adsorption: Isotherm, kinetic and thermodynamic studies. *J. Hazard. Mater.* **2019**, *371*, 146−155.
(26) Bing, R.; Ke, W.; Baoshui, Z.; Hanyu, L.; Yuzhong, N.; Hou, C.; Zhenglong, Y.; Xuzhao, L.; Huaqing, Z. Adsorption behavior of PAMAM dendrimers functionalized silica for Cd(II) from aqueous solution: Experimental and theoretical calculation. *J. Taiwan Inst. Chem. Eng.* **2019**, *101*, 80−91.
(27) Weijun, S.; Dandan, W.; Zetao, Z.; Zhenning, L.; Ying, X.; Yu, F. Synthesis of Schiff base-functionalized silica for effective adsorption of Re(VII) from aqueous solution. *J. Taiwan Inst. Chem. Eng.* **2019**, *100*, 277−284.
(28) Dobrzyńska, J.; Dobrowolski, R.; Olchowski, R.; Zięba, E.; Barczak, M. Palladium adsorption and preconcentration onto thiol- and amine-functionalized mesoporous silicas with respect to analytical applications. *Microporous Mesoporous Mater.* **2019**, *274*, 127−137.
(29) Bagheri, S.; Amini, M. M.; Behbahani, M.; Rabiee, G. Low cost thiol-functionalized mesoporous silica, KIT-6-SH, as a useful adsorbent for cadmium ions removal: A study on the adsorption isotherms and kinetics of KIT-6-SH. *Microchem. J.* **2019**, *145*, 460−469.
(30) El-Massaoudi, M.; Radi, S.; Bacquet, M.; Degoutin, S.; Garcia, Y. Highly efficient and selective adsorbent for potentially toxic metals removal from aquatic media. *J. Environ. Chem. Eng.* **2018**, *6*, 5980−5989.
(31) Tighadouini, S.; Radi, S.; Anannaz, M.; Bacquet, M.; Degoutin, S.; Tillard, M.; Eddike, D.; Amhamdi, H.; Garcia, Y. Engineering *β*-ketoenol structure functionality in hybrid silica as excellent adsorbent material for removal of heavy metals from water. *New J. Chem.* **2018**, *42*, 13229−13240.
(32) Tighadouini, S.; Radi, S.; Elidrissi, A.; Zaghrioui, M.; Garcia, Y. Selective Confinement of Cd^{I} in Silica Particles Functionalized with *β*-Keto-Enol-Bisfuran Receptor: Isotherms, Kinetic and Thermodynamic Studies. *Eur. J. Inorg. Chem.* **2019**, 3180−3186.
(33) Giret, S.; Hu, Y.; Masoumifard, N.; Boulanger, J.-F.; Estelle Juère, E.; Kleitz, F.; Larivière, D. Selective Separation and Preconcentration of Scandium with Mesoporous Silica. *ACS Appl. Mater. Interfaces* **2018**, *10*, 448−457.
(34) Tighadouini, S.; Radi, S.; Elidrissi, A.; Haboubi, K.; Bacquet, M.; Degoutin, S.; Zaghrioui, M.; Garcia, Y. Removal of toxic heavy metals from river water samples using a porous silica surface modified with a new *β*-ketoenolic host. *Beilstein J. Nanotechnol.* **2019**, *10*, 262−273.
(35) Tighadouini, S.; Radi, S.; Ferbinteanu, M.; Garcia, Y. Highly Selective Removal of Pb(II) by a Pyridylpyrazole-*β*-ketoenol Receptor Covalently Bonded onto the Silica Surface. *ACS Omega* **2019**, *4*, 3954−3964.
(36) Hughes, D. L.; Afsar, A.; Harwood, L. M.; Jiang, T.; Laventine, D. M.; Shaw, L. J.; Hodson, M. E. Adsorption of Pb and Zn from binary metal solutions and in the presence of dissolved organic carbon by DTPA-functionalised, silicacoated magnetic nanoparticles. *Chemosphere* **2017**, *183*, 519−527.
(37) Zhang, X.; Zhang, Y.; Zhang, X.; Li, S.; Huang, Y. Nitrogen rich core-shell magnetic mesoporous silica as an effective adsorbent for removal of silver nanoparticles from water. *J. Hazard. Mater.* **2017**, *337*, 1−9.
(38) Radi, S.; Abiad, C. E.; Moura, N. M. M.; Faustino, M. A. F.; Neves, M. G. P. M. S. New Hybrid Adsorbent Based on Porphyrin Functionalized Silica for Heavy Metals Removal: Synthesis, Characterization, Isotherms, Kinetics and Thermodynamics Studies. *J. Hazard. Mater.* **2019**, *370*, 80−90.
(39) Radi, S.; El Massaoudi, M.; Bacquet, M.; Degoutin, S.; Adarsh, N. N.; Robeyns, K.; Garcia, Y. A novel environment-friendly hybrid material based on chemical modified silica gel with a bispyrazole derivative for the removal of Zn^{II}, Pb^{II}, Cd^{II} and Cu^{II} traces from aqueous solutions. *Inorg. Chem. Front.* **2017**, *4*, 1821−1831.
(40) Radi, S.; Tighadouini, S.; Bacquet, M.; Degoutin, S.; Janus, L.; Mabkhot, Y. N. Fabrication and Covalent Modification of Highly Chelate Hybrid Material Based on Silica-Bipyridine Framework for Efficient Adsorption of Heavy Metals: Isotherms, Kinetics and Thermodynamics Studies. *RSC Adv.* **2016**, *6*, 82505−82514.
(41) Radi, S.; El Abiad, C.; Carvalho, A. P.; Santos, S. M.; Faustino, M. A. F.; Neves, M. G. P. M. S.; Moura, N. M. M. An efficient hybrid adsorbent based on silica-supported amino penta-carboxylic acid for water purification. *J. Mater. Chem. A* **2018**, *6*, 13096−13109.
(42) Tighadouini, S.; Radi, S.; Bacquet, M.; Degoutin, S.; Zaghrioui, M.; Jodeh, S.; Warad, I. Removal efficiency of Pb(II), Zn(II), Cd(II) and Cu(II) from aqueous solution and natural water by ketoenol−pyrazol receptor functionalized silica hybrid adsorbent. *Sep. Sci. Technol.* **2017**, *52*, 608−621.
(43) Radi, S.; El-Massaoudi, M.; Benaissa, H.; Adarsh, N. N.; Ferbinteanu, M.; Devlin, E.; Sanakis, Y.; Garcia, Y. Crystal Engineering of a Series of Complexes and Coordination Polymers Based on Pyrazole-Carboxylic Acid Ligands. *New J. Chem.* **2017**, *41*, 8232−8241.
(44) Radi, S.; Yahyi, A.; Ettouhami, A.; Chaudhary Jha, A.; Adarsh, N. N.; Robeyns, K.; Garcia, Y. Synthesis and Crystal Structures of Mononuclear Cu^{II}/Co^{II} Coordination Complexes from Pyrazole-Dicarboxylate Acid Derivatives. *Polyhedron* **2015**, *85*, 383−388.
(45) Kowalik, M.; Masternak, J.; Kazimierczuk, K.; Khavryuchenko, O. V.; Barszcz, B. Lead(II) coordination polymers with imidazole-4- and pyrazole-3-carboxylate isomeric linkers: Structural diversity and luminescence properties. *J. Solid State Chem.* **2018**, *266*, 100−111.
(46) Guerrero, M.; Calvet, T.; Font-Bardia, M.; Pons, J. Synthesis and Characterization of Pd (II), Pt(II), Cu(I), Ag(I) and Cu(II) Complexes with N,O-Hybrid Pyrazole Ligand. *Polyhedron* **2016**, *119*, 555−562.
(47) Najar, A. M.; Tidmarsh, I. S.; Ward, M. D. Lead(II) Complexes of Bis-and Tris-Bidentate Compartmental Ligands Based on Pyridyl-Pyrazole and Pyridyl-Triazole Fragments: Coordination Networks and a Discrete Dimeric Box. *CrystEngComm* **2010**, *12*, 3642−3650.
(48) Ahumada, G.; Fuentealba, M.; Roisnel, T.; Kahlal, S.; Córdova, R.; Carrillo, D.; Saillard, J.-Y.; Hamon, J.-R.; Manzur, C. Spectroscopic, structural, electrochemical and computational studies

https://dx.doi.org/10.1021/acsomega.0c01616
ACS Omega 2020, 5, 17324−17336

of some new 2-thienyl-containing β-diketonate complexes of cobalt-(II), nickel(II) and copper(II). *J. Mol. Struct.* **2017**, *1150*, 531−539.
(49) Hui, Y.-Y.; Shu, H.-M.; Hu, H.-M.; Song, J.; Yao, H.-L.; Yang, X.-L.; Wu, Q.-R.; Yang, M.-L.; Xue, G.-L. Syntheses, structures and magnetic properties of tetranuclear and trinuclear nickel(II) complexes with β-diketone-functionalized pyridinecarboxylate ligand. *Inorg. Chim. Acta* **2010**, *363*, 3238−3243.
(50) Sánchez, I.; Cuerva, C.; Marcelo, G.; Oliveira, E.; Santos, H. M.; Campo, J. A.; Lodeiro, C.; Cano, M. Designing Eu-β-diketonate complexes as a support of ionic liquid crystals (ILCs) with additional luminescent properties. *Dyes Pigm.* **2018**, *159*, 395−405.
(51) Liu, X.; Hamon, J.-R. Recent developments in penta-, hexa- and heptadentate Schiff base ligands and their metal complexes. *Coord. Chem. Rev.* **2019**, *389*, 94−118.
(52) Li, H.; Xi, D.; Niu, Y.; Wang, C.; Xu, F.; Liang, L.; Xu, P. Design, synthesis and biological evaluation of cobalt(II)-Schiff base complexes as ATP-noncompetitive MEK1 inhibitors. *J. Inorg. Biochem.* **2019**, *195*, 174−181.
(53) Bernadette Amali, I.; Kesavan, M. P.; Vijayakumar, V.; Indra Gandhi, N.; Rajesh, J.; Rajagopal, G. Structural analysis, antimicrobial and cytotoxic studies on new metal(II) complexes containing N_2O_2 donor Schiff base ligand. *J. Mol. Struct.* **2019**, *1183*, 342−350.
(54) Sing, K. S. W.; Everett, D. H.; Haul, R. A. W.; Moscou, L.; Pierotti, R. A.; Rouquerol, J.; Siemienie wska, T. Reporting physisorption data for gas/solid systems with special reference to the determination of surface area and porosity (IUPAC Recommendations 1984). *Pure Appl. Chem.* **1985**, *57*, 603−619.
(55) Sales, J. A. A.; Airoldi, C. Calorimetric investigation of metal ion adsorption on 3-glycidoxypropyltrimethylsiloxanepropane-1,3-diamine immobilized on silica gel. *Thermochim. Acta* **2005**, *427*, 77−83.
(56) Sales, J. A. A.; Faria, F. P.; Prado, A. G. S.; Airoldi, C. Attachment of 2-aminomethyl- pyridine molecule onto grafted silica gel surface and its ability in chelating cations. *Polyhedron* **2004**, *23*, 719−725.
(57) Nandi, B. K.; Goswami, A.; Purkait, M. K. Adsorption characteristics of brilliant green dye on kaolin. *J. Hazard. Mater.* **2009**, *161*, 387−395.
(58) Largitte, L.; Pasquier, R. A Review of the Kinetics Adsorption Models and Their Application to the Adsorption of Lead by an Activated Carbon. *Chem. Eng. Res. Des.* **2016**, *109*, 495−504.
(59) Xiao, Y.; Azaiez, J.; Hill, J. M. Erroneous Application of Pseudo-Second-Order Adsorption Kinetics Model: Ignored Assumptions and Spurious Correlations. *Ind. Eng. Chem. Res.* **2018**, *57*, 2705−2709.
(60) Chen, X. Modeling of experimental adsorption isotherm data. *Information* **2015**, *6*, 14−22.
(61) Krishni, R. R.; Foo, K. Y.; Hameed, B. H. Adsorption of methylene blue onto papaya leaves: comparison of linear and nonlinear isotherm analysis. *Desalin. Water Treat.* **2014**, *52*, 6712−6719.
(62) Zhang, H.; Dang, Q.; Liu, C.; Yu, D.; Wang, Y.; Pu, X.; Liu, Y.; Liang, Y.; Cha, D. Fabrication of Methyl Acrylate and Tetraethylenepentamine Grafted Magnetic Chitosan Microparticles for Capture of Cd(II) from Aqueous Solutions. *J. Hazard. Mater.* **2019**, *366*, 346−357.
(63) Chamorro, E.; Pérez, P.; Domingo, L. R. On the nature of Parr functions to predict the most reactive sites along organic polar reactions. *Chem. Phys. Lett.* **2013**, *582*, 141−143.
(64) Weinhold, F.; Landis, C. R. Natural Bond orbitals and extensions of localized bonding concepts. *Chem. Educ.: Res. Pract. Eur.* **2001**, *2*, 91−104.
(65) Hu, J.; Wang, X.; Liu, L.; Wu, L. A facile and general fabrication method for organic silica hollow spheres and their excellent adsorption properties for heavy metal ions. *J. Mater. Chem. A* **2014**, *2*, 19771−19777.
(66) He, S.; Zhao, C.; Yao, P.; Yang, S. Chemical modification of silica gel with multidentate ligands for heavy metals removal. *Desalin. Water Treat.* **2016**, *57*, 1722−1732.
(67) Moftakhar, M. K.; Dousti, Z.; Yaftian, M. R.; Ghorbanloo, M. Investigation of heavy metal ions adsorption behavior of silica-supported Schiff base ligands. *Desalin. Water Treat.* **2016**, *57*, 27396−27408.
(68) Zhang, M.; Zhang, Z.; Liu, Y.; Yang, X.; Luo, L.; Chen, J.; Yao, S. Preparation of core−shell magnetic ion-imprinted polymer for selective extraction of Pb(II) from environmental samples. *Chem. Eng. J.* **2011**, *178*, 443−450.
(69) Guo, B.; Deng, F.; Zhao, Y.; Luo, X.; Luo, S.; Au, C. Magnetic ion-imprinted and -SH functionalized polymer for selective removal of Pb(II) from aqueous sample. *Appl. Surf. Sci.* **2014**, *292*, 438−446.
(70) Fan, H.-T.; Sun, X.-T.; Zhang, Z.-G.; Li, W.-X. Selective removal of lead (II) from aqueous solution by an ion-imprinted silica sorbent functionalized with chelating N-donor atoms. *J. Chem. Eng. Data* **2014**, *59*, 2106−2114.
(71) Faur-Brasquet, C.; Kadirvelu, K.; Le Cloirec, P. Removal of Metal Ions from Aqueous Solution by Adsorption onto Activated Carbon Cloths: Adsorption Competition with Organic Matter. *Carbon* **2002**, *40*, 2387−2392.
(72) Rahman, M.; Adil, M.; Yusof, A.; Kamaruzzaman, Y.; Ansary, R. Removal of Heavy Metal Ions with Acid Activated Carbons Derived from Oil Palm and Coconut Shells. *Materials* **2014**, *7*, 3634−3650.
(73) Kołodyńska, D.; Krukowska, J.; Thomas, P. Comparison of Sorption and Desorption Studies of Heavy Metal Ions from Biochar and Commercial Active Carbon. *Chem. Eng. J.* **2017**, *307*, 353−363.
(74) Xue, X.; Li, F. Removal of Cu(II) from aqueous solution by adsorption onto functionalized SBA-16 mesoporous silica. *Microporous Mesoporous Mater.* **2008**, *116*, 116−122.
(75) Kohn, W.; Sham, L. J. Self-Consistent Equations Including Exchange and Correlation Effects. *Phys. Rev.* **1965**, *140*, A1133−A1138.
(76) Bader, R. F. W. *Atoms in Molecules: A Quantum Theory*; Clarendon Press; Oxford, U.K., 1994.
(77) Pastorczak, E.; Corminboeuf, C. Perspective: Found in translation: Quantum chemical tools for grasping non-covalent interactions. *J. Chem. Phys.* **2017**, *146*, 120901−120913.
(78) Frisch, M. J.; Trucks, G. W.; Schlegel, G. B.; et al. *Gaussian 09*, Revision A.02; Gaussian Inc.: Wallingford, 2009.
(79) Lu, T.; Chen, F. Multiwfn: A multifunctional wavefunction analyser. *J. Comput. Chem.* **2012**, *33*, 580−592.
(80) Lee, C.; Yang, W.; Parr, R. G. Development of the Colle-Salvetti correlation-energy formula into a functional of the electron density. *Phys. Rev. B: Condens. Matter Mater. Phys.* **1988**, *37*, 785.
(81) Wiberg, K. B. Ab Initio Molecular Orbital Theory by W. J. Hehre, L. Radom, P. v. R. Schleyer, and J. A. Pople, John Wiley, New York, 548pp. Price: $79.95 (1986). *J. Comput. Chem.* **1986**, *7*, 379.
(82) Hay, P. J.; Wadt, W. R. Ab initio effective core potentials for molecular calculations. Potentials for the transition metal atoms Sc to Hg. *Chem. Phys.* **1985**, *82*, 270.
(83) Gonohe, N.; Abe, H.; Mikami, N.; Ito, M. Two-color photoionization of van der Waals complexes of fluorobenzene and hydrogen-bonded complexes of phenol in supersonic jets. *J. Phys. Chem.* **1985**, *89*, 3642−3648.
(84) Gutowski, M.; Chal/asiński, G. Critical evaluation of some computational approaches to the problem of basis set superposition error. *J. Chem. Phys.* **1993**, *98*, 5540−5554.
(85) Altomare, A.; Cascarano, G.; Giacovazzo, C.; Guagliardi, A. SIR92 − a program for automatic solution of crystal structures by direct methods. *J. Appl. Crystallogr.* **1993**, *26*, 343−350.
(86) Sheldrick, G. M. Crystal structure refinement with SHELXL. *Acta Crystallogr., Sect. A: Found. Crystallogr.* **2008**, *64*, 112−122.
(87) *Crystal Structure 4.2: Crystal Structure Analysis Package*; Rigaku Corporation: Tokyo, Japan 196-8666, 2000−2015.

https://dx.doi.org/10.1021/acsomega.0c01616
ACS Omega 2020, 5, 17324−17336